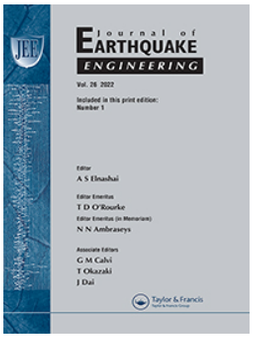

Journal of Earthquake Engineering

ISSN: (Print) (Online) Journal homepage: https://www.tandfonline.com/loi/ueqe20

The Strongest Possible Earthquake Ground Motion

Igor A. Beresnev

To cite this article: Igor A. Beresnev (2022) The Strongest Possible Earthquake Ground Motion, Journal of Earthquake Engineering, 26:1, 563-572, DOI: 10.1080/13632469.2019.1691681

To link to this article: https://doi.org/10.1080/13632469.2019.1691681

Published online: 21 Nov 2019.

JOURNAL OF EARTHQUAKE ENGINEERING
2022, VOL. 26, NO. 1, 563–572
https://doi.org/10.1080/13632469.2019.1691681

Taylor & Francis
Taylor & Francis Group

The Strongest Possible Earthquake Ground Motion

Igor A. Beresnev

Department of Geological & Atmospheric Sciences, Iowa State University, Ames, Iowa, USA

ABSTRACT

Ground accelerations have been seen to exceed three accelerations of gravity (*g*). Can extreme motions further surpass this level as more earthquakes are experienced? Also, ground shaking of nearly same severity has been observed near earthquakes differing in magnitude by three units. Does this imply independence of extreme shaking on magnitude? Calculations based on the representation theorem of elasticity verify that maximum ground accelerations on bedrock even for the greatest magnitudes saturate at the level of approximately 3 *g*. Maximum ground velocities approach the values of 2 m/s. Also, the peak level of extreme shaking is nearly independent of magnitude.

ARTICLE HISTORY
Received 15 December 2018
Accepted 6 November 2019

KEYWORDS
Extreme ground motion; representation theorem; earthquake-radiation modeling; ground accelerations; ground velocities

1. Introduction

The loss of life during earthquakes is primarily caused by the collapse of a built environment. By Newton's second law of motion, forcing on structures is caused by ground acceleration. Accelerations and velocities are among the important parameters of ground motion from the practical standpoint, which, for the benefit of future generations and the success of earthquake-resistant building design, should be constrained by the seismological science.

Prior to the 1971 San Fernando, California earthquake, it was commonly thought that the peak (maximum) ground acceleration could not exceed half of *g*, where *g* is the acceleration of gravity (Reiter 1990, Figure 7.1). However, a vertical acceleration of 2.1 g was recorded during the M_w (moment magnitude) 6.8 1985 Nahanni event in Northwest Territories, Canada, and a horizontal value of 1.8 *g* was documented at the Tarzana site, within the greater Los Angeles area, during the M_w 6.7 1994 Northridge earthquake. The seismological and engineering communities were taken aback again when an acceleration of 2.2 *g* was observed during the relatively modest M_w 6.3 2011 Christchurch, New Zealand event. Still further, several locations exhibited peak accelerations exceeding 2 *g* during the M_w 9.0 2011 Tohoku, Japan earthquake. Finally, the much weaker M_w 6.9 2008 Iwate-Miyagi event in Japan produced an unprecedented vertical motion of 3.9 *g* (Aoi, Kunugi, and Fujiwara 2008). More examples of extreme shaking, prior to 2007, are provided by Anderson (2010).

Two questions emerge from the limited observational evidence available to date. First, there seems to be a trend toward saturation of maximum ground motions at the level of about 3–4 *g*, depending on the site conditions. Is this tendency real, or is it simply because

CONTACT Igor A. Beresnev beresnev@iastate.edu Department of Geological and Atmospheric Sciences, Iowa State University, 253 Science I, 2237 Osborn Drive, Ames, Iowa 50011-3212

we have not seen an even greater event yet (Strasser and Bommer 2009)? Second, working against the latter conclusion is the fact that the level of extreme ground motions does not seem to depend on the magnitude. Indeed, nearly three magnitude units (the difference in radiated seismic energy close to $32^3 \approx 33000$ times) separate the New Zealand earthquake from the Japan event, and yet the ground accelerations were nearly the same. Does this fact imply that the magnitude is not the main parameter controlling the extreme shaking?

Can these two fundamental observations be explained by a single earthquake model, which could then also suggest the answer to the question of vital engineering and societal significance, "What is the maximum ground motion possible?"

2. The Earthquake-Radiation Model

The numerical simulations of extreme ground motions, both kinematic and dynamic, have so far been accomplished through the solution of equations of motion, achievable on rare and expensive parallel machines, and are limited to relatively low frequencies, typically below 10 Hz. Examples are provided by Beresnev (2017b), who emphasized the use of the representation theorem of elasticity as an under-utilized rigorous means for establishing the upper bounds on high-frequency seismic motions, at any frequency. The following computational model was established.

The representation theorem provides the exact mathematical solution for earthquake radiation from a rupturing fault. For a rupture in a homogeneous space, the ith component of the radiated displacement wavefield $u_i(\mathbf{x}, t)$ is

$$u_i(\mathbf{x},t) = \frac{\mu}{4\pi\rho}\iint\left[\frac{c_{1i}}{R^4}\int_{R/\alpha}^{R/\beta} t'\Delta u(\boldsymbol{\xi}, t-t')dt' + \frac{c_{2i}}{\alpha^2R^2}\Delta u\left(\boldsymbol{\xi}, t-\frac{R}{\alpha}\right)\right.$$
$$\left. - \frac{c_{3i}}{\beta^2R^2}\Delta u\left(\boldsymbol{\xi}, t-\frac{R}{\beta}\right) + \frac{c_{4i}}{\alpha^3R}\Delta \dot{u}\left(\boldsymbol{\xi}, t-\frac{R}{\alpha}\right) - \frac{c_{5i}}{\beta^3R}\Delta \dot{u}\left(\boldsymbol{\xi}, t-\frac{R}{\beta}\right)\right] d\Sigma(\boldsymbol{\xi}), \tag{1}$$

where $\Delta u(\boldsymbol{\xi}, t)$ is the displacement (slip) function on the fault (the source time function), $\Delta \dot{u}(\boldsymbol{\xi}, t)$ is its time derivative (the slip rate), R is the distance from a point $\boldsymbol{\xi}$ on the fault plane to the observation point $\mathbf{x}$; α, β, μ, ρ are the P- and S-wave propagation speeds, shear modulus, and density of the medium, and c_{1i}, c_{2i}, … are purely geometrical dimensionless coefficients dependent on $\boldsymbol{\xi}$ and $\mathbf{x}$ only. The double integration is over the fault plane $\Sigma(\boldsymbol{\xi})$ (Aki and Richards 2002, equation 10.39). Here we also use the explicit compact convolution integral in the first term in the integrand instead of introducing the long notation through the function $F(t)$ as in the original equation (10.39) of Aki and Richards (Beresnev 2017b, Equations 1 and A1-A2).

In the far field, the Fourier spectra of the radiated displacement are commonly observed to follow the "ω^{-2}" functional shape (where ω is the angular frequency), in which the spectrum is flat below the characteristic ("corner") frequency ω_c and falls off as ω^{-2} above (Aki 1967; Beresnev and Atkinson 1997; Boore 1983; Brune 1970). The analytical form of the source time function that leads to the ω^{-2} spectrum in the far field is

$$\Delta u(t) = \begin{cases} 0, & t<0 \\ U\left[1-\left(1+\frac{t}{\tau}\right)e^{-t/\tau}\right], & t \geq 0 \end{cases} \tag{2}$$

(Beresnev and Atkinson 1997, equation 6), where the parameter τ determines how fast the fault dislocation rises to its final value U. If v_{max} is the maximum velocity of the rise, the parameter τ is

$$\tau = \frac{U}{ev_{\max}}, \tag{3}$$

where e is the base of the natural logarithm (Beresnev 2001, 398). The corner frequency is $1/\tau$. The quantities U and v_{max} are the two fundamental physical parameters that control the form of the displacement on the fault.

With the assumption that the fault rupture propagates radially outward from its hypocentral initiation point, $\Delta u(\boldsymbol{\xi}, t) = \Delta u(t - r/v_r)$, where r is the distance along the fault plane and v_r is the rupture-propagation velocity, the integrand in (1) becomes completely defined.

3. Computation of Maximum Ground Motions

The integral (1) was evaluated numerically. The hypocenter was placed in the center of a vertical rectangular right-lateral strike-slip fault. The elastic constants are taken as: α = 5 km/s, $\beta = \alpha/\sqrt{3}$, ρ = 2600 kg/m^3, $v_r = 0.8\beta$.

Ground acceleration, as the high-frequency measure of earthquake shaking, is controlled by the frequencies above ω_c. The modulus of the Fourier spectrum of acceleration in the high-frequency range is $a_{hf}(\omega) = CM_0\omega_c^2$, where C is a constant and M_0 is the scalar seismic moment (e.g., Boore 1983, Equations 1–3). Using the definition of the moment, $M_0 = \mu UA$, where A is the fault area, and Equation (3) leads to

$$a_{hf} = CA\mu e^2 \frac{v_{\max}^2}{U}. \tag{4}$$

Equation (4) shows that the parameter v_{max} is the one primarily responsible for the values of ground acceleration. This relation strictly applies to the seismic radiation in the far field only, where the fault can be treated as a point source. However, its comparison with the high-frequency levels of acceleration spectra computed using the exact integral (1) by Beresnev (2017a) showed that Equation (4) is accurate in the near field as well, as is theoretically justified (Beresnev 2017a, 1283).

Beresnev and Atkinson (2002), based on the ω^{-2} model of earthquake radiation, inferred the variability in v_{max} for all well-recorded significant earthquakes in North America in the range from 0.25 to 0.60 m/s. Anil-Bayrak and Beresnev (2009) obtained the variability in v_{max} from about 0.2 to 2 m/s by the direct application of relation (3) to recorded spectra, as well as from literature review. This coincides with the range inferred from literature sources by Rowe and Griffith (2015, Fig. 2). Aki and Richards (2002, 502) indicate the limited range in the observed slip velocities from 0.1 to 1 m/s. Still another independent estimate in setting the maximum possible value of v_{max} comes from the analysis of the data for stress drop, a formal parameter often used to quantify the strength of high-frequency radiation. For both major (Kanamori and Anderson 1975, Fig. 2) and small (Scholz 2002, Figure 4.10) earthquakes, stress drop does not appear to exceed 400 bars. Beresnev (2001, equation 19) derived a formula for the conversion of the stress drop to the maximum slip velocity, from which the value of 400 bars corresponds to $v_{max} \approx$

2 m/s. To summarize, there is presently no observational evidence that the slip rate on earthquake faults can exceed 2 m/s, without any magnitude dependence either, which is the fact that may be fundamentally rooted in the restrictions imposed by the friction forces between the sliding faces of the faults. The parameter v_{max} has been set to 2 m/s in the calculation of maximum ground motion.

Since up to three time differentiations are involved in the calculation of the acceleration time histories from displacement using integral (1), resulting in considerable enhancement in high-frequency numerical noise, the double integration was carried out to the high precision of eight digits. This places significant demand on computer time; for example, obtaining one component of wave displacement for an M_w 6 earthquake requires approximately 54 h on a modern multi-processor PC. This time increases progressively for larger earthquakes: for an M_w 7 fault, the corresponding computing time is about 96 h. The main calculations were performed for an M_w 6 earthquake on a 10 by 10 km fault, the area being prescribed by its empirical relation with a moment magnitude of Wells and Coppersmith (1994, Table 2(a)). Once the moment magnitude and the area have been set, the modeled constant offset U follows from combining the definition of M_0 and that of the moment magnitude, $M_w = (2/3)\log M_0 - 10.7$. For the M_w 6 scenario earthquake, U = 0.49 m. To account for the free-surface effect, all resulting waveforms were amplified by a factor of two (Boore 1983, 1871).

The ground-motion simulation algorithm used was fully described and validated by modeling the near-fault records at the Lucerne Valley station during the M_w 7.2 1992 Landers, California earthquake by Beresnev (2017b).

A scaling relation can be established from (4) that allows extending the peak accelerations computed for an M_w 6 event to greater earthquakes. Using the definitions of the seismic moment, the moment magnitude, and the empirical relation $\log U = -4.80 + 0.69M_w$ of Wells and Coppersmith (1994, Table 2(b)) ($M_w > 5.6$), Equation (4) yields

$$a_{hf} = 10^{18.65} C e^2 (1.26^{M_w}) v_{max}^2, \tag{5}$$

where the SI units have been preserved.

The scaling relation (4) applies to ground-acceleration values because of their control by the high-frequency spectra. On the other hand, the ground displacement is defined by the low-frequency spectra, while the velocity lies in between. We can only hypothesize that the same scaling applies to ground velocity, although this conjecture will be tested in the simulations.

In the computations, the offset U over the fault plane was assumed constant. There is no mechanism by which the heterogeneity in the slip distribution could systematically control the amplitudes of high-frequency radiation, the maximum slip velocity being the dominant factor (Beresnev 2003, 2451, 2017a). This is seen from Equation (5), in which, as long as M_w (an integral measure of slip) is constant, there is no effect of slip distribution, no matter uniform or irregular, over the fault area, whereas v_{max} carries a quadratic effect.

The lack of control of fault roughness on the spectral content of ground motions was directly demonstrated by Beresnev (2017a) through the same direct integration of (1) as in the present work. Specifically, randomly disturbing the uniform slip and the maximum slip rate or introducing asperities did not lead to any appreciable differences in the shape of radiated Fourier spectra. A theoretical justification was provided. The study also showed theoretically

that the variable rupture speed could modify the fault directivity but could not cause any systematic effect on the preferential generation of high frequencies.

4. Results

Figure 1 exhibits the map view of the vertical fault (solid line) and the two perpendicular profiles (dashed lines) on which ground motions were calculated. The distances indicated are in meters measured from the upper corner of the fault (not to scale). The fault length

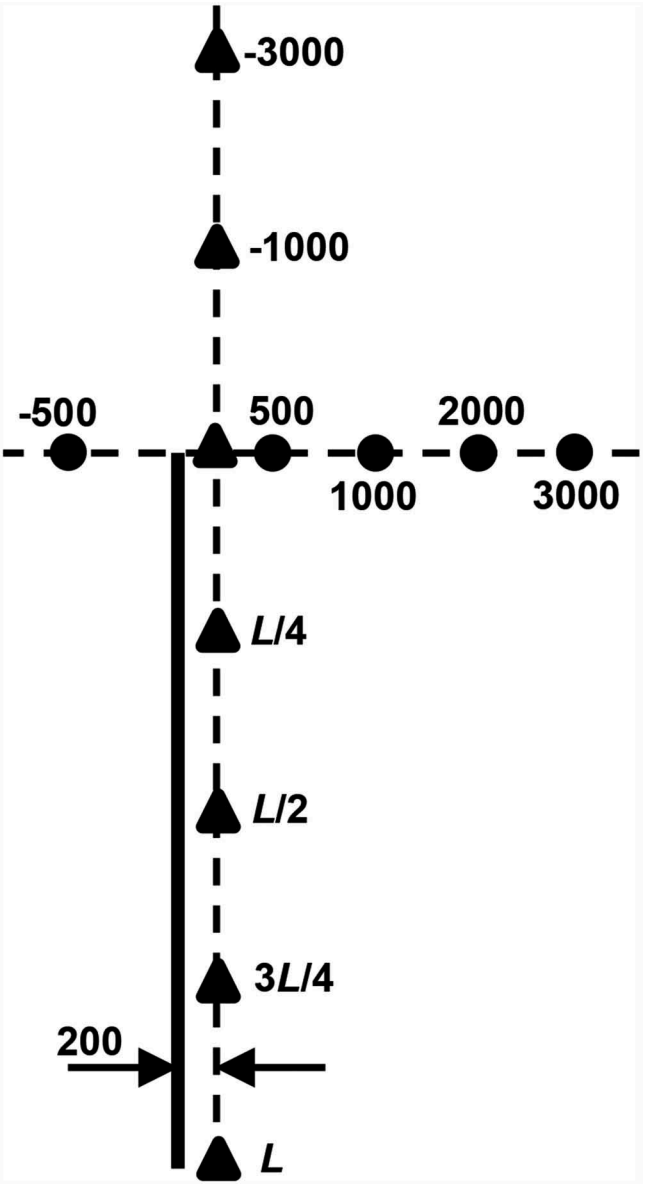

Figure 1. Layout of the profiles.

is L, and the horizontal plane of the profiles is 200 m above the upper edge of the fault. The observation lines were chosen to address the directivity effects.

Figure 2 shows the ground-displacement, velocity, and acceleration waveforms along the two profiles for the fault-normal component, which, of the three components of motion, produced the greatest accelerations. The respective distances and moduli of peak ground velocities (PGV) and accelerations (PGA) (in units of g) are indicated. For the fault-normal component, the distribution of waveforms is antisymmetric with respect to the distance of $0.5L$ for the parallel profile, and the point at $0.5L$ is the node. For the perpendicular profile, the waveforms are symmetric with respect to the fault line. The antisymmetric and symmetric parts are not shown.

The highest velocity and acceleration are 0.86 m/s and 1.01 g at 0 m on the parallel profile. Equation (5) allows extension of the acceleration result to the greatest magnitudes

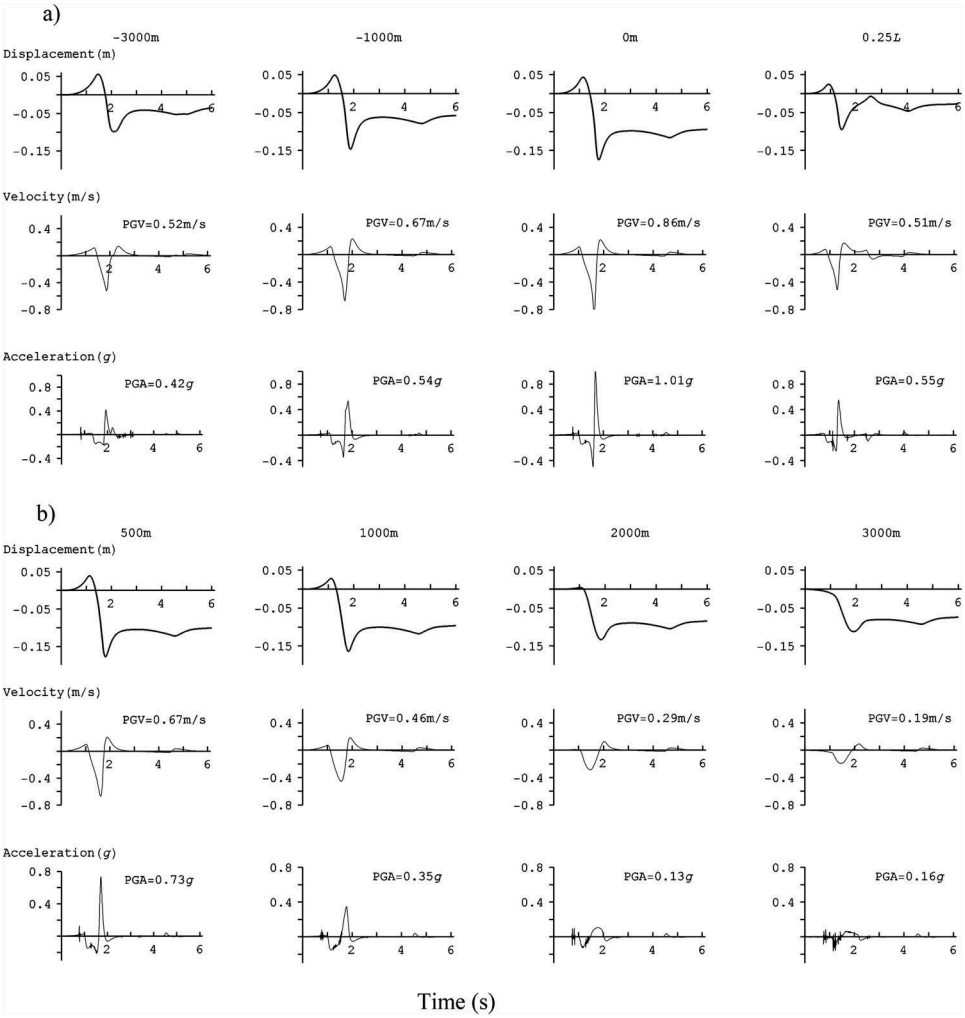

Figure 2. Ground displacements, velocities, and accelerations along the parallel (a) and perpendicular (b) profiles.

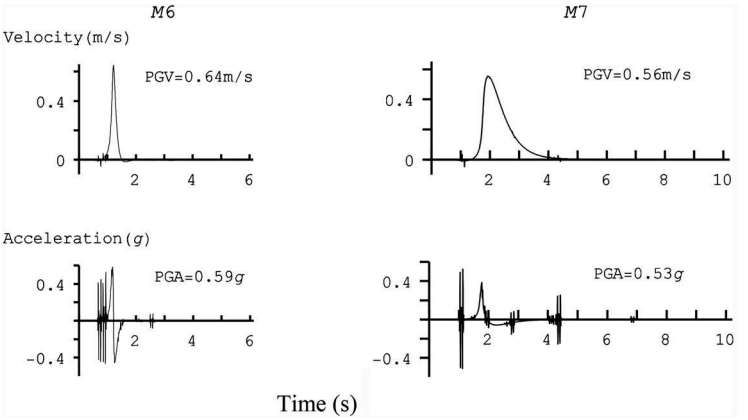

Figure 3. Velocigrams and accelerograms for M_w 6 and 7 earthquakes.

possible. For example, the value obtained for an M_w 6 earthquake will be multiplied by the factor of approximately $1.26^3 \approx 2.0$ to yield one for an M_w 9 event, giving the maximum possible acceleration of approximately 2.0 g. The extreme accelerations during earthquakes are thus very weakly dependent on the magnitude. If the same scaling applies to velocity, its maximum plausible value will be approximately 1.7 m/s.

Figure 3 verifies this point for both ground velocity and acceleration. It shows velocigrams and accelerograms computed for a fault-parallel component at the distance $L/2$ on the parallel profile for an M_w 6 and an M_w 7 events. The PGV and PGA are virtually unchanged, despite the magnitude difference of one unit.

All conclusions remain valid for a vertical dip-slip fault, as it can be obtained from a strike-slip fault by renaming the coordinate axes.

5. Discussion

The inferences of this study apply to a hard-rock condition and can be considered as establishing a cap on the maximum seismic input to the bottom of a local soil profile. Amplification by soft sediments and three-dimensional surface and subsurface topography may cause further increase in ground acceleration beyond the established limits. The additional near-surface amplification by low-velocity deposits is normally expected to be significantly reduced at the level of extreme ground motions by nonlinear elastic behavior of soil materials (Beresnev and Wen 1996; Field *et al.* 1997). For example, as documented by Field *et al.* (1997, Fig. 2), the seismic amplification by sediments in the Los Angeles basin, normally up to a factor of three during smaller earthquakes, was reduced to less than two during the strong shaking caused by the Northridge event. However, when conventional amplification raises the amplitude in the vertical component beyond 1 g, spikes of extremely high positive accelerations are possible due to ground spalling. This effect, known in explosion seismology, was shown to be responsible for the exceptional shaking, approaching 4 g at the surface, at the site IWTH25 during the Iwate-Miyagi event. The downhole accelerometer, located at the depth of 260 m in soft rock (β = 1810 m/s), recorded a relatively modest 0.7 g in the same vertical component (Aoi,

Kunugi, and Fujiwara 2008). Further conventional amplification took place in the upper layers. The top 34 m of the profile was composed of river-terrace deposits. Then, in the negative acceleration phases, part of the near-surface ground separated, was thrown into the air, and underwent a period of free fall, producing sharp acceleration spikes upon landing. The latter were referred to as the "slapdown" phases by Yamada, Mori, and Heaton (2009).

Clearly, the occurrence of spalling and the resulting slapdown phases should be taken into account when predicting extreme ground motions in the vertical component on soft grounds. A quantitative model of spalling, developed by Beresnev (2019), shows that, for the maximum hypothesized input to a soil profile of 3 g, the peak acceleration in the spikes due to ground separation can reach the level of 7 g. This value should be considered as an estimate of the maximum possible acceleration on the surface of soft deposits.

Our conclusions are also predicated on the assumption that in-situ velocities at which the faults slip do not exceed 2 m/s. Factors fundamentally limiting this value may be fault friction or rheology of the material surrounding the fault. It is also conceivable that owing to irregular fault topography, kinetic energy is constantly expended on the destruction of the roughness on the rupture surface. It is not our intention to speculate about a particular cause but to simply point out that there is no observational evidence that the velocities may be greater.

Duan and Day (2010) inferred peak ground velocities of up to 5 m/s in extreme motions using a computational dynamic model of earthquake rupture. Unlike our kinematic simulation, whose parameters are generally better observationally constrained, the dynamic theoretical models have the disadvantage of having to specify numerous, insufficiently known parameters of faulting, such as the state of initial stress or idealized constitutive laws for dynamic and static friction. In the absence of direct empirical evidence, these parameters are often prescribed in a near-arbitrary manner. In addition, Duan and Day (2010) simulated a two-dimensional line rupture, to which no magnitude can be assigned. The authors themselves recognize the limitations of their model, stating that their calculated PGVs will generally be larger than in 3D models (Duan and Day 2010, 3017). This may explain the discrepancy existing between our study and theirs.

It is worth mentioning in this regard that a collateral result of our study is that near-fault maximum ground velocities are on the same order as the fault slip rate itself (cf. the ground velocity maximum of 0.86 m/s in Fig. 2 with the value of the parameter v_{max} of 2 m/s in the computations). Had the extreme slip rates much in excess of 2 m/s been the norm in nature, they would have been seen in near-fault instrumental records obtained on rock. No such facts are presently known (Anderson 2010), although the data are scarce. Our conclusions may need to be revised if compelling evidence is encountered that fault slip rates can exceed 2 m/s.

6. Conclusions

Calculations using an exact analytical method, quantitatively validated on the near-fault records from the 1992 Landers earthquake, show that the trend toward the saturation of extreme accelerations at the levels below 3 g on bedrock is real. The maximum possible ground velocities approach the values of 2 m/s. Albeit seemingly counterintuitive, the peak ground accelerations and velocities are nearly independent of magnitude. This explains

why shaking of the same severity was experienced during both the M_w 6.3, New Zealand and M_w 9.0, Japan events. The practical difference that an earthquake of greater magnitude will make, relative to a smaller one, is that, due to a significantly increased rupture size, a much larger area will experience near-fault extreme motions, and the shaking will be of longer duration.

The maximum achievable rate of slip on the fault controls the level of the resulting high-frequency shaking. In the prediction of maximum possible ground accelerations and velocities, therefore, imposing a cap on the realistically realizable slip velocity is the most important task. Immediate field observations of faulting are exceptionally rare. Research should continue on constraining the value of v_{max} using all available direct and indirect means.

7. Data and Resources

No data were used in the paper. All inferences were made through the numerical evaluation of the representation integral (1) as described.

Acknowledgments

The author is indebted to two anonymous reviewers for constructive comments.

References

Aki, K. 1967. Scaling law of seismic spectrum. *Journal of Geophysical Research* 72: 1217–31. doi: 10.1029/JZ072i004p01217.

Aki, K., and P. G. Richards. 2002. *Quantitative seismology*. 2nd ed. Sausalito, CA: University Science Books.

Anderson, J. G. 2010. Source and site characteristics of earthquakes that have caused exceptional ground accelerations and velocities. *Bulletin of the Seismological Society of America* 100: 1–36. doi: 10.1785/0120080375.

Anil-Bayrak, N. A., and I. A. Beresnev. 2009. Fault slip velocities inferred from the spectra of ground motions. *Bulletin of the Seismological Society of America* 99: 876–83. doi: 10.1785/0120080008.

Aoi, S., T. Kunugi, and H. Fujiwara. 2008. Trampoline effect in extreme ground motion. *Science* 322: 727–30. doi: 10.1126/science.1163113.

Beresnev, I. A. 2001. What we can and cannot learn about earthquake sources from the spectra of seismic waves. *Bulletin of the Seismological Society of America* 91: 397–400. doi: 10.1785/0120000115.

Beresnev, I. A. 2003. Uncertainties in finite-fault slip inversions: To what extent to believe? (A critical review). *Bulletin of the Seismological Society of America* 93: 2445–58. doi: 10.1785/0120020225.

Beresnev, I. A. 2017a. Factors controlling high-frequency radiation from extended ruptures. *The Journal of Seismology* 21: 1277–84. doi: 10.1007/s10950-017-9660-6.

Beresnev, I. A. 2017b. Simulation of near-fault high-frequency ground motions from the representation theorem. *Pure and Applied Geophysics* 174: 4021–34. doi: 10.1007/s00024-017-1623-x.

Beresnev, I. A. 2019. *Calculation of extreme accelerations in earthquake motion due to ground spalling*. (in review).

Beresnev, I. A., and G. M. Atkinson. 1997. Modeling finite-fault radiation from the ω^n spectrum. *Bulletin of the Seismological Society of America* 93: 67–84.

Beresnev, I. A., and G. M. Atkinson. 2002. Source parameters of earthquakes in eastern and western North America based on finite-fault modeling. *Bulletin of the Seismological Society of America* 92: 695–710. doi: 10.1785/0120010101.

Beresnev, I. A., and K.-L. Wen. 1996. Nonlinear soil response – A reality? *Bulletin of the Seismological Society of America* 86: 1964–78.

Boore, D. M. 1983. Stochastic simulation of high-frequency ground motions based on seismological models of the radiated spectra. *Bulletin of the Seismological Society of America* 73: 1865–94.

Brune, J. N. 1970. Tectonic stress and the spectra of seismic shear waves from earthquakes. *Journal of Geophysical Research* 75: 4997–5009. doi: 10.1029/JB075i026p04997.

Duan, B., and S. M. Day. 2010. Sensitivity study of physical limits on ground motion at Yucca Mountain. *Bulletin of the Seismological Society of America* 100: 2996–3019. doi: 10.1785/0120090372.

Field, E. H., P. A. Johnson, I. A. Beresnev, and Y. Zeng. 1997. Nonlinear ground-motion amplification by sediments during the 1994 Northridge earthquake. *Nature* 390: 599–602. doi: 10.1038/37586.

Kanamori, H., and D. L. Anderson. 1975. Theoretical basis of some empirical relations in seismology. *Bulletin of the Seismological Society of America* 65: 1073–95.

Reiter, L. 1990. *Earthquake hazard analysis*. New York: Columbia University Press.

Rowe, C. D., and W. A. Griffith. 2015. Do faults preserve a record of seismic slip: A second opinion. *Journal of Structural Geology* 78: 1–26. doi: 10.1016/j.jsg.2015.06.006.

Scholz, C. H. 2002. *The mechanics of earthquakes and faulting*. 2nd ed. Cambridge, UK: Cambridge University Press.

Strasser, F. O., and J. J. Bommer. 2009. Strong ground motions – Have we seen the worst? *Bulletin of the Seismological Society of America* 99: 2613–37. doi: 10.1785/0120080300.

Wells, D. L., and K. J. Coppersmith. 1994. New empirical relationships among magnitude, rupture length, rupture width, rupture area, and surface displacement. *Bulletin of the Seismological Society of America* 84: 974–1002.

Yamada, M., J. Mori, and T. Heaton. 2009. The slapdown phase in high-acceleration records of large earthquakes. *Seismological Research Letters* 80: 559–64. doi: 10.1785/gssrl.80.4.559.